ISSN 0015-4628, Fluid Dynamics, 2025, Vol. 60:170. © Pleiades Publishing, Ltd., 2025.
Russian Text © The Author(s), 2025, published in Fiziko-Khimicheskaya Kinetika v Gazovoi Dinamike, 2025, Vol. 26, No. 1.

Effect of Tetrahedral Mesh Characteristics on the Accuracy of Modeling Supersonic Flow past an Axisymmetric Model

I. A. Shirokov[a,*] and T. G. Elizarova[b]

[a] *Moscow State University, Faculty of Computational Mathematics and Cybernetics, Moscow, Russia*

[b] *Keldysh Institute of Applied Mathematics, Moscow, Russia*

******e-mail: ivanshirokov@inbox.ru*

Received November 1, 2025; revised November 10, 2025; accepted November 10, 2025

Abstract—The effect of parameters of unstructured tetrahedral meshes on the results of simulation of viscous, heat-conducting gas flow past the standard HB-2 model at zero angle of attack and the Mach number equal to 1.5 is studied. The computational meshes are constructed using the freely available TetGen and Gmsh packages. The simulation is based on a system of regularized (quasi-gasdynamic) equations. It is shown that using the meshes that are superior in a combination of criteria (small cell size on the model surface, low degree of non-uniformity, high quality of cells) gives the simulation results closer to experimental data than using the meshes with inferior characteristics. Moreover, improving the mesh quality makes it possible to simulate unsteady flow regimes.

Keywords: tetrahedral mesh, mesh generators, HB-2 model, quasi-gas dynamic algorithm

DOI: 10.1134/S0015462825603791

1. INTRODUCTION

For the numerical modeling of gas- and hydrodynamic flows in three-dimensional domains, the finite volume method is widely used to approximate the macroscopic equations on computational meshes that cover the region under consideration. A common type of such meshes are unstructured tetrahedral meshes, for whose generation numerous mathematical approaches [1–4] and software packages, including freely distributed ones [5–7], have been developed. In addition to the characteristics of the finite-difference algorithm, the quality of numerical modeling is largely determined by the quality of the mesh used. In [8], the effect of the quality of meshes with cells of various shapes on the resolution of the shock wave front in supersonic flow past a blunt body was studied and a conclusion was made about a significant effect of the cell shape and the degree of meshes non-uniformity on the simulation results. It was shown that uniform meshes with cubic cells have an advantage among the considered meshes.

As a whole, the computational meshes must satisfy conflicting requirements, namely, they must not have an excessively large number of elements, their generation must not require significant computational time, the meshes must not be too coarse and must have sufficiently high-quality elements (in this work, tetrahedrons). The first two requirements are determined by the power of available computing systems. The characteristic size of the elements and their quality (defined as a measure of their deviation from a regular tetrahedron) affect the accuracy of approximation of the equations and, in the end, the accuracy of simulation of the physical processes. As the size of elements decreases and their quality improves, the number of nodes and the computer time required for mesh generation increase (it should be considered that generating high-quality cells requires the use of optimization algorithms).

In practice, compromise approaches are used. In particular, in modeling gas-dynamic flows, mesh refinement is used in "important" parts of the computational domain (boundary layer, shock waves, etc.). In such cases, the resulting mesh is non-uniform, which can negatively impact the quality of simulation. Studying the effect of mesh parameters (characteristic cell size, degree of non-uniformity, and cell quality) on the accuracy of modeling the physical processes is of great interest from the standpoint of selecting the optimum mesh generation methods for specific problems.

In this study, the effect of unstructured tetrahedral mesh parameters is examined using the example of modeling external supersonic (Mach number Ma = 1.5) viscous heat-conducting gas flow past an axisym-

metric standard HB-2 model [9–12] with the reference center body diameter $D = 0.1$ m at zero angle of attack and the Reynolds number $\mathrm{Re}_D = 2\times10^5$.

The quasi-gas dynamic (QGD) algorithm, that approximates the quasi-gas dynamic equations on spatial meshes and then solves the initial boundary value problem [13–15], is used as the mathematical model. The quasi-gas dynamic equations are regularized gas dynamics equations. Regularization is based on the assumption that the mass flux density differs from the average momentum per unit volume by a small amount. The form of dissipative additives that arise under this assumption can be obtained either by using a kinetic model or by averaging the initial equations over a small spatial-temporal interval. The equations constructed in this way are closely related to the original system of gas dynamics equations written in the form of the mass, momentum, and total energy conservation laws, and ensure nondecreasing thermodynamic entropy of the system. An additional dissipation inherent in the quasi-gas dynamic equations increases their computational stability and makes it possible to use a conditionally stable, time-explicit finite-difference scheme with approximation of all spatial derivatives by central differences without introducing additional limiters.

The first version of the quasi-gas dynamic equations and examples of modeling the problem of flow past a plate in comparison with the Navier–Stokes model and calculations using the direct Monte Carlo simulation methods were given in [16]. It was subsequently shown that the quasi-gas dynamic algorithm is a fairly universal tool for studying the features of gas-dynamic flows in subsonic and supersonic regimes [17–20]. The experience in numerical calculations has shown the advantages of quasi-gas dynamic algorithms in modeling unsteady flows, including direct simulation of turbulent flows at low Reynolds numbers [18]. The possibility of modeling unsteady flows in the base region behind a body within the framework of quasi-gas dynamic equations depends on the computational mesh and is investigated in the present study.

The particular implementation of the quasi-gas dynamic algorithm corresponds to [19, 20]. Unstructured tetrahedral meshes constructed using the freely available TetGen [21] and Gmsh [22] mesh generators are used. The results obtained in calculations on various meshes are compared with the data obtained in experimental studies of HB-2 models in wind tunnels [9–11]. A comparison of the results makes it possible to draw conclusions about the importance of various characteristics of computational meshes in terms of improving the accuracy of gas-dynamic flow simulation, as well as the possibility of simulating unsteady flow regimes.

2. DESCRIPTION AND ANALYSIS OF THE MESHES USED

The open-source mesh generators TetGen (version 1.5) and Gmsh (version 4.9.3) are used to construct the meshes. Both generators make it possible to construct unstructured tetrahedral meshes in a given three-dimensional domain, the characteristic mesh step being adjustable within the domain boundaries. The generator algorithms are based on Delaunay triangulation.

To construct a mesh using the TetGen generator, an original algorithm for constructing a surface mesh used as the input data for the TetGen generator was developed [23]. To launch the TetGen generator, the command tetgen.exe-pq1.4/17a0.00007Y hb2.poly was used. The options are as follows: -p to create a tetrahedral mesh, -q to optimize the mesh (optimization parameters: 1.4 is the maximum ratio of the radius of the sphere circumscribed around the tetrahedron to the minimum edge, and 17 is the minimum dihedral angle of the tetrahedron in degrees), -a sets the maximum volume of the tetrahedron, and -Y saves the surface mesh specified in the hb2.poly file.

The Gmsh mesh generation technology follows the methodology described in [7]: using the Gmsh-integrated computer-aided design (CAD) system, a geometric description of the HB-2 model (hb2.geo file), which is used as the input data for mesh generation, is constructed. Generation in Gmsh is carried out interactively with default parameters, using the Frontal-Delaunay algorithm for surface mesh generation, the Delaunay algorithm for volume mesh generation, and also using cell quality optimization (the Gmsh optimization algorithm).

The meshes were generated on personal computers; the generation time for a single mesh was not greater than 10 min. In Table 1 we have given characteristics of the generated meshes.

Here, *hm* is the characteristic linear size of cells on the model surface, and *hd* is the maximum characteristic linear size of cells on the outer boundary of the computational domain. These quantities are specified as parameters in constructing the mesh.

For all meshes, the computational domains are axisymmetric. For meshes **3**–**6**, the computational domains are the same and have the shape of a fragment of ellipsoid. For meshes **1** and **2**, the computa-

Table 1. Characteristics of computational meshes

Mesh	Generator	Number of cells	*hm*, m	*hd*, m	Ratio of the max and min cell dimensions, approximately
1	TetGen	806108	0.002	0.05	50
2	TetGen	2587192	0.001	0.05	100
3	Gmsh	365714	0.008	0.04	5
4	Gmsh	2871822	0.004	0.02	5
5	Gmsh	6753696	0.003	0.015	5
6	Gmsh	7857823	0.008	0.008	1

tional domains have the shape of a truncated cone and are close in size. In Fig. 1 we have reproduced the general view of meshes **2** and **4** in the axial cross-section.

The last column of Table 1 yields the approximate ratio between the maximum and minimum linear cell sizes. This ratio can serve as a measure of mesh non-uniformity. The authors of [7] argue that it is undesirable when this ratio is greater than 10. For a more detailed estimate of the degree of mesh non-uniformity, in Fig. 2 we have reproduced the specific distributions of the tetrahedral cell sizes: the minimum (on the left) and maximum (on the right) cell edge lengths. The curve labeling corresponds to Table 1. The abscissas of the markers *m* (model) and *d* (domain) denote the characteristic mesh sizes *hm* and *hd*, given in Table 1.

Table 1 and the distributions plotted in Fig. 2 clearly show that meshes **1** and **2** are much more non-uniform than meshes **3**–**6**. This is partly due to the larger difference between the specified characteristic dimensions on the boundaries of the model and the computational domain for meshes **1** and **2**, and partly due to the difference in the algorithms: the TetGen generator, by default, creates a tetrahedral mesh with a strong refinement toward the model and domain boundaries (i.e., with a coarseness away from boundaries). On the contrary, the Gmsh generator, by default, constructs an approximately uniform tetrahedral mesh. Moreover, if different mesh steps are specified on different domain boundaries, the spatial mesh step varies uniformly from one boundary to the other.

Generating meshes with small *hm* and low nonuniformity leads to a significant increase in the number of mesh cells, and, consequently, to increase in computational difficulties. Therefore, the generated meshes are a compromise in order to maintain a moderate number of cells.

To estimate the quality of the meshes used, we will consider the weight (by the number of cells) distributions of the quality criterion of a tetrahedral cell *q* (Fig. 3). The quality criterion is calculated as

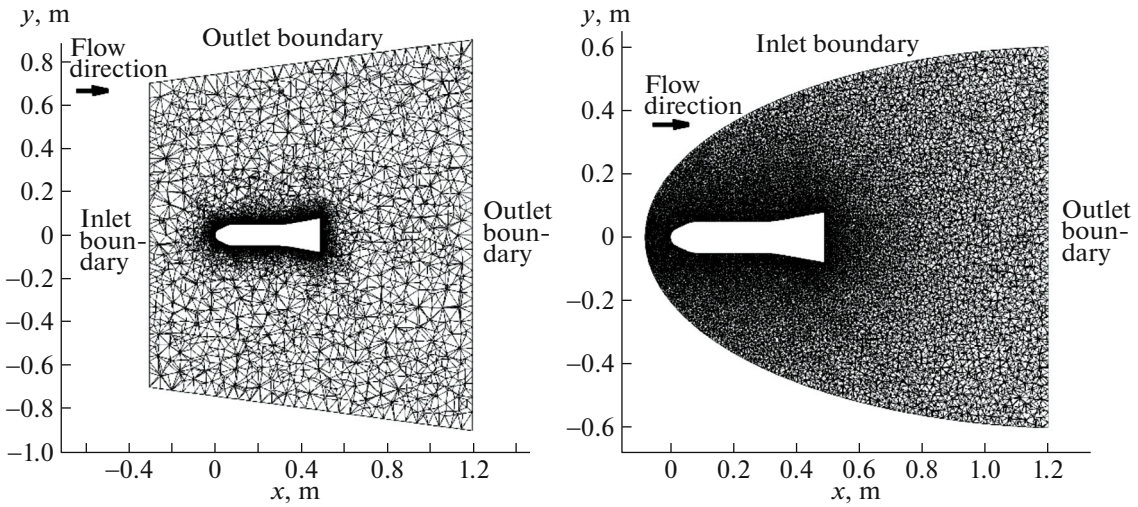

Fig. 1. Cross-section of the computational meshes **2**, in the left, and **4**, in the right, at $z = 0$, and the location of the boundaries.

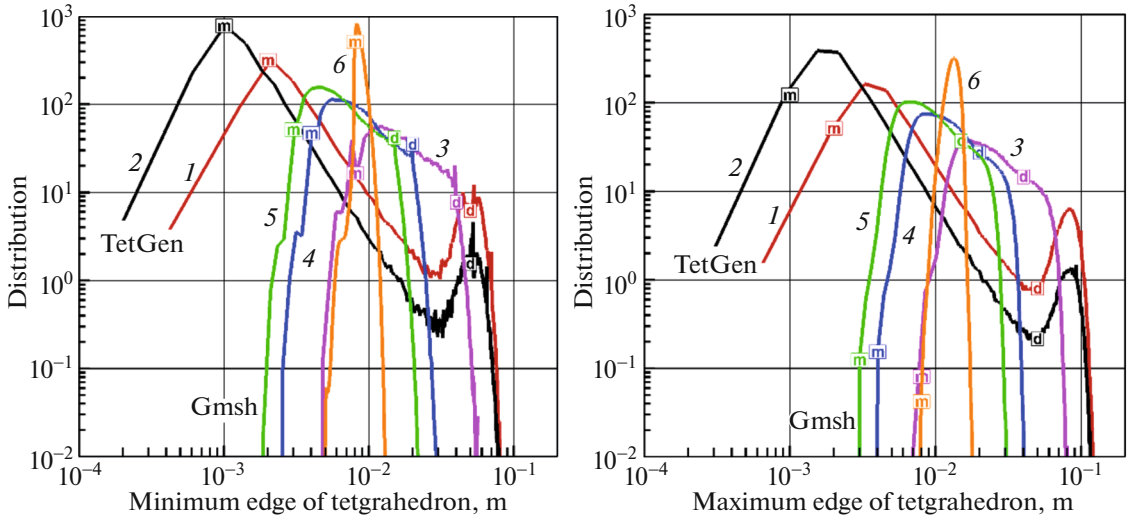

Fig. 2. Cell size distributions: minimum (on the left) and maximum (in the right) lengths of the cell edge for the constructed meshes. Markers denote the characteristic mesh step specified on the model surface and on the domain boundary. The numbering of curves corresponds to Table 1.

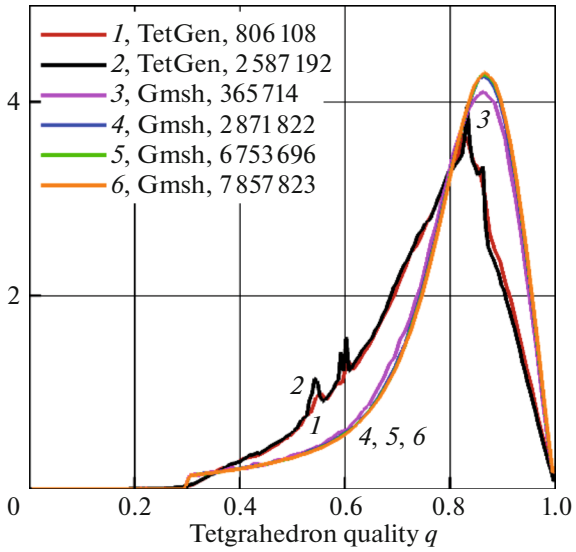

Fig. 3. Quality criterion distributions of tetrahedral cells of the meshes used with indication of the mesh generators and the number of cells. The numbering of curves corresponds to Table 1.

$q = 3r/R$, where r is the radius of the sphere inscribed in the tetrahedron and R is the radius of the sphere circumscribed around the tetrahedron [7]. In the case of a regular tetrahedron, $q = 1$, otherwise $q < 1$. As q decreases, the tetrahedral cell becomes more "irregular" and, accordingly, "poor" from the point of view of the accuracy of approximation of the macroscopic equations. In Fig. 3, the distributions are normalized so that the area under each curve is equal to unity. If the mesh contains a larger number of "good" cells (with a large q), then its distribution curve is located to the right. It is evident that meshes **1** and **2** have similar distributions, while for meshes **3**–**6** the distributions almost coincide. Thus, the distribution of q depends only slightly on the given characteristic mesh size and the number of cells, and is determined by the TetGen and Gmsh algorithms.

We can distinguish three mesh properties important for the simulation accuracy: the characteristic cell size on the model surface *hm* (Table 1), the degree of non-uniformity (Table 1 and Fig. 2), and the cell quality determined by the distribution of the parameter q (Fig. 3). Mesh **2** is the best for the parameter *hm*,

and mesh **6** is the best for the degree of non-uniformity. Meshes **3**–**6** have some advantage over mesh **1** and **2** in terms of cell quality. Mesh **5** is the best for the totality of parameters.

3. SIMULATION ALGORITHM

The basis of the quasi-gas dynamic algorithm is the system of quasi-gas dynamic equations for an ideal polytropic gas [13–15]:

$$\frac{\partial}{\partial t}\rho + \nabla_i j_m^i = 0,$$
$$\frac{\partial}{\partial t}\rho u^j + \nabla_i \left(j_m^i u^j\right) + \nabla^j p = \nabla_i \Pi^{ij}, \tag{1}$$
$$\frac{\partial}{\partial t}E + \nabla_i \left(j_m^i H\right) + \nabla_i q^i = \nabla_i \left(\Pi^{ij} u_j\right).$$

Here, ρ is the density, u^i are the components of the macroscopic velocity, $p = \rho RT$ is the pressure, T is the temperature, $E = \rho u^2/2 + p/(\gamma - 1)$ is the total energy per unit volume, $H = (E + p)/\rho$ is the total specific enthalpy, the adiabatic index (specific heat ratio) for air is $\gamma = 1.4$. The expressions for the mass flux density vector j_m^i, the viscous stress tensor Π^{ij}, and the heat flux q^i can be written as follows:

$$j_m^i = \rho\left(u^i - w^i\right), \quad w^i = (\tau/\rho)\left(\nabla_j \rho u^i u^j + \nabla^i p\right),$$
$$\Pi^{ij} = \Pi_{\mathrm{NS}}^{ij} + \tau u^i \rho\left(u_k \nabla^k u^j + \left(\frac{1}{\rho}\right)\nabla_j p\right) + \tau\delta^{ij}\left(u_k \nabla^k p + \gamma p \nabla^k u_k\right),$$
$$\Pi_{\mathrm{NS}}^{ij} = \mu\left(\nabla^i u^j + \nabla^j u^i - (2/3)\,\delta^{ij}\nabla^k u_k\right) + \zeta\delta^{ij}\nabla^k u_k,$$
$$q^i = q_{\mathrm{NS}}^i - \tau u^i \rho\left(u_j \nabla^j \varepsilon + p u_j \nabla^j (1/\rho)\right), \quad q_{\mathrm{NS}}^i = -\kappa\nabla^i T. \tag{2}$$

In this case $\varepsilon = p/(\rho(\gamma - 1))$ is the internal energy per unit mass of gas, Π_{NS}^{ij} and q_{NS}^i are the viscous stress tensor and the heat flux in the system of Navier–Stokes equations, μ, ζ, and κ are the shear and bulk viscosity and thermal conductivity coefficients, respectively.

The shear viscosity coefficient μ is calculated using the temperature dependence

$$\mu = \mu_0 (T/T_0)^{\omega}, \tag{3}$$

where μ_0 is the gas viscosity at the free-stream flow temperature T_0, $\omega = 0.74$ is the exponent of intermolecular interaction. The thermal conductivity coefficient is calculated as $\varkappa = \mu R\gamma/(\mathrm{Pr}(\gamma - 1))$, where for air the Prandtl number $\mathrm{Pr} = 0.737$. The coefficient τ, that determines additional dissipation in the quasi-gas dynamic algorithm, is defined as

$$\tau = \mu/(p\mathrm{Sc}) + \alpha h/c, \tag{4}$$

where the first term relates to the shear viscosity coefficient and is of the order of the characteristic time between gas particle collisions. The second term provides an additional artificial viscosity to ensure the stability of the quasi-gas dynamic algorithm when simulating supersonic dense gas flows. The magnitude of this artificial additive is determined by the tuning parameter $\alpha = 0.5$, where h is the characteristic local size of the spatial cell, c is the local speed of sound, and $\mathrm{Sc} = 0.799$ is the Schmidt number for air.

The bulk viscosity coefficient is lso represented in the form of two terms, the first term is an approximation formula, and the second term introduces additional artificial viscosity, also to increase the stability of the algorithm in supersonic regions:

$$\varsigma = \mu\left(\left(\frac{5}{3}\right) - \gamma\right) + \delta\left(\frac{h}{c}\right)p. \tag{5}$$

Here, as in (4), the magnitude of the regularizing additive is determined by the local parameters h and c and the tuning parameter $\delta = 3$.

In [20], the numerical modeling methodology is described. The gasdynamic parameters (density, velocity, pressure, temperature, and energy) are reduced to dimensionless form. The characteristic length

of 1 m, the density, and the speed of sound in the free-stream flow are taken as the dimensional parameters. Thus, in the free-stream flow $\rho = 1$, $p = 1/\gamma$, $T = 1$, $U = \mathrm{Ma}$, and $\mathrm{Re}_D = \mathrm{Ma}D/\mu_0$. In dimensionless variables, the equation of state takes the form $p = \rho T/\gamma$ and the speed of sound is $c = \sqrt{T}$.

The values of gas-dynamic parameters are determined at mesh nodes. At points of the computational domain located between mesh nodes the values of gas-dynamic variables are determined as the arithmetic mean of the values at the nodes. The finite-difference approximation of the macroscopic quasi-gas dynamic equations is constructed using the control volume method. The barycentric control volume is constructed around each mesh node. Since the dissipation coefficients depend on local parameters, the algorithm has a first-order spatial approximation on the tetrahedral mesh.

Initially, the free-stream parameters are specified on the inlet boundary. The same parameters are specified inside the computational domain (except for the velocity: the gas is initially stationary there). On the inlet boundary, the free-stream values are maintained constant. On the outlet boundary, soft conditions, that allow the gas to freely leave the domain, are imposed. On the rigid boundary of the model the no-slip conditions are imposed (the velocity vector is equal to zero), an additional boundary condition of the quasi-gas dynamic algorithm being used: the normal derivative of the pressure is equal to zero. On the rigid boundary of the model, the conditions are assumed to be adiabatic. The configuration of the inlet and outlet boundaries differs for the TetGen and Gmsh meshes and is shown in Fig. 1.

For the mesh analogues of system (1)–(5), the solution to the initial boundary value problem is found using a time-explicit finite-difference scheme with the first-order time approximation. The time step is calculated as $h_t = \beta h/c$, where $\beta = 0.1$ is the Courant number, and h and c are the same local parameters as those in (4)–(5). The calculations were performed using the K-100 hybrid supercomputer installed in the Super-Computer Center of Collective Usage of the Keldysh Institute of Applied Mathematics of the Russian Academy of Sciences [24]. Parallel computations based on decomposition of the computational domain using the MPI standard and the METIS library were used. Depending on the calculation variant, the computing time ranged from 1 h to several days when using from 64 to 128 processor cores.

4. COMPARISON OF THE SIMULATION RESULTS

Using the described algorithm, viscous heat-conducting gas flow past the standard HB-2 model was simulated using meshes **1**–**6** at $\mathrm{Ma} = 1.5$ and $\mathrm{Re}_D = 2\times10^5$. The three-dimensional distributions of gas-dynamic parameters were studied at dimensionless time t ranging from 9 to 25 (the number of iterations of the finite-difference scheme was of the order of 10^5–10^6). By the instant $t = 9$, a physically adequate flow pattern was formed in all variants. Calculations from $t = 9$ to 25 were carried out to study the unsteady regime.

As an example, in Fig. 4 we have reproduced the flow patterns obtained on meshes **2** and **4** at $t = 9$. On mesh **2**, the flow is stationary, with a toroidal vortex forming behind the base surface. On mesh **4**, the flow behind the base surface is unsteady, with formation of a chaotic vortex pattern. Shock waves at a distance from the model are better resolved on mesh **4**.

To estimate the accuracy of gas-dynamic flow simulation, we consider the following criteria:

– accordance of the obtained stagnation parameters on the forebody of the model with theoretical data calculated on the basis of the Hugoniot conditions and isentropic formulas [14];

– possibility of obtaining the non-steady-state flow pattern;

– accordance of the aerodynamic total and forebody axial force coefficients obtained by integrating the pressure distribution over the surface of the model with the experimental values;

– accordance of the obtained surface pressure profiles in the axial cross-section with experimental data;

– convergence of the results when refining the mesh;

– resolution of shock waves at a distance from the model.

We will now estimate the effect of the mesh parameters (see Table 1) on the simulation accuracy according to the specified criteria.

In Fig. 5 (on the left) we have compared the obtained dimensionless stagnation parameters with theoretical data. It can be seen that the minimum deviation from theory is achieved on mesh **5**, which is the best for the totality of parameters. A comparison of results **1** and **2** shows convergence of the results when refining the TetGen meshes, but satisfactory agreement with theory is not achieved even on mesh **2**. A comparison of results **3**, **4**, and **5** shows convergence in refining the Gmsh meshes. There is no satisfac-

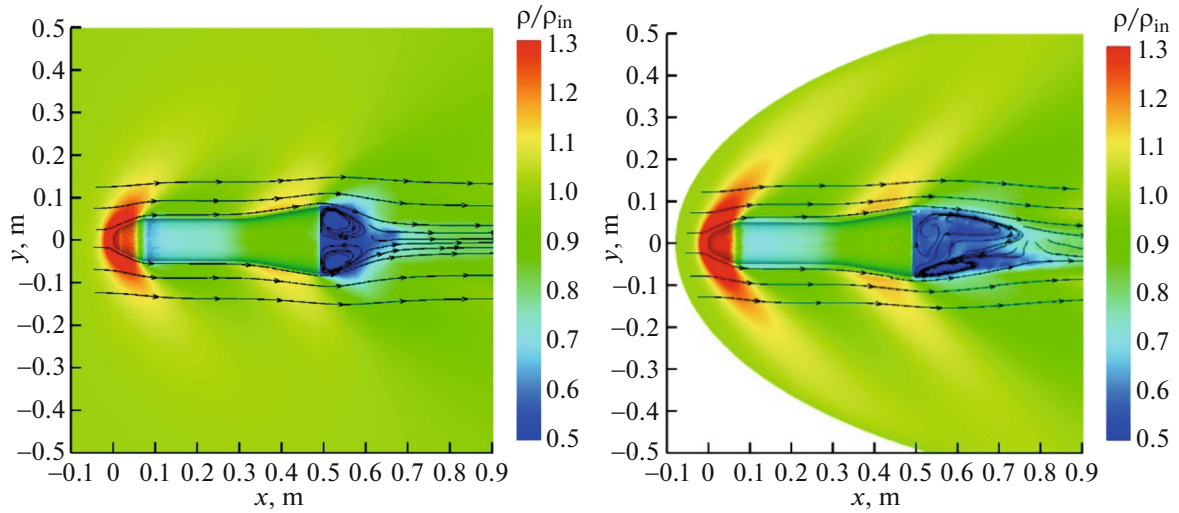

Fig. 4. Normalized density levels and streamlines at $z = 0$, obtained by modeling on meshes **2** (on the left) and **4** (on the right).

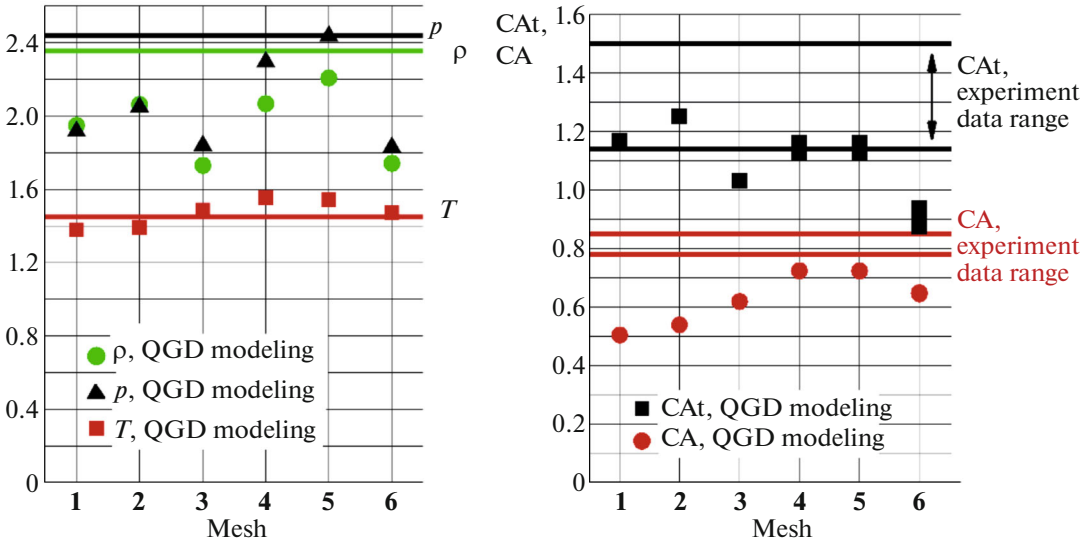

Fig. 5. Dimensionless stagnation parameters, simulation and theory (on the left); aerodynamic coefficients, simulation and experiment (on the right).

tory agreement on the mesh with large *hm* **3**. There is also no agreement on the mesh **6**, which is close to uniform over the entire computational domain, but with large *hm*.

It turned out that the unsteady regime with formation of chaotic vortices behind the model's base region can be obtained only using meshes **4**, **5**, and **6**. Apparently, the presence of excessively large cells in meshes **1**, **2**, and **3** increases the effective viscosity of the simulation algorithm. This impedes obtaining the unsteady solution. The effect of non-stationarity on the stagnation parameters is insignificant and is not reflected in Fig. 5.

In Fig. 5 (on the right) we have compared the obtained aerodynamic total and forebody axial force coefficients *CAt* and *CA* (*CAt* = *CA* + *CAb*, where *CAb* is the axial force coefficient) with the experimental values [9–11]. Since the authors of the experimental studies provide slightly different measurement data (in particular, this is associated with the difficulty of measuring *CAb* under the influence of the support sting), Fig. 5 shows the ranges of known experimental values (between horizontal lines). Satisfactory agreement with the experiment is achieved on meshes **4** and **5**. Meshes **1** and **2** ensure good agreement

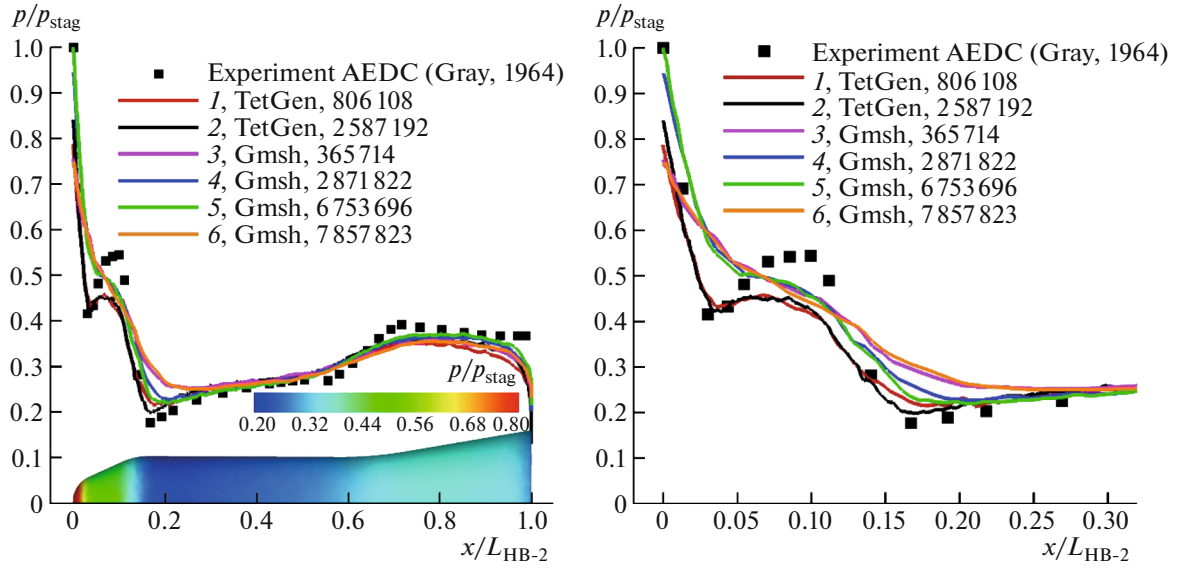

Fig. 6. Surface pressure profiles in the $z = 0$ cross-section: experiment and simulation on various meshes (on the left, along the entire model; on the right, an enlarged view of the nose fragment). The pressure levels on the model surface correspond to mesh **5**. The curve notation corresponds to Figs. 2 and 3.

for the total axial force coefficient *CAt*, but the values of *CA* do not correspond to experiment. Refining the Gmsh mesh (compare **3** and **4**, **5**) brings the results closer to experiment. There is no agreement with experiment on the coarse but nearly uniform mesh **6**. Since the flow regime on meshes **4**, **5**, and **6** is unsteady, the corresponding markers are elongated in the vertical direction, reflecting small variations in *CAt* over time. These variations in *CA* are small and not reflected in Fig. 7.

Note that in most experimental studies of the HB-2 model in wind tunnels, the Reynolds number Re_D is of the order of 1.5×10^6 at Ma = 1.5, whereas in the present study, to improve the stability of the calculations, we used $\mathrm{Re}_D = 2\times10^5$. However, in [9], the data showing that in experiments the effect of the Reynolds number in the range from 2×10^5 to 1.4×10^6 on the aerodynamic coefficients is insignificant at moderate Mach numbers (Ma < 4) were presented. Furthermore, on mesh **4**, we have carried out a calculation at $\mathrm{Re}_D = 1.4\times10^6$, which exactly corresponds to the conditions in [9]. There are almost no differences from the $\mathrm{Re}_D = 2\times10^5$ variant. Thus, our comparison of the simulation results at $\mathrm{Re}_D = 2\times10^5$ with experimental data at the greater Re_D is justified.

In Fig. 6 we have reproduced the surface pressure profiles in the cross-section $z = 0$, obtained in modeling on the constructed meshes, and the corresponding experimental data from [9]. The pressure is normalized to the theoretical stagnation pressure at the nose of the model. In general, the best agreement with the experiment is observed on mesh **5**, while the results on mesh **4** are somewhat worse. However, on these meshes, the pressures are overestimated at local minima, and the stepwise nature of the profile is not resolved at $0.05 < x/L_{\mathrm{HB-2}} < 0.1$. On meshes **1** and **2**, the stepwise section is partially resolved, and there is an agreement with the experiment at local minima, but at local maxima the pressure values are noticeably lower than the experimental ones. Convergence of the calculation results to the experiment is observed when refining the TetGen (comparison of **1** and **2**) and Gmsh (comparison of **4** and **5**) meshes. On meshes **3** and **6**, which are coarse on the model surface, the profiles are further from the experiment than those on the finer meshes **1**, **2**, **4**, and **6**.

The resolution of shock waves with growth of the distance from the model depends on the cell size in this region and is best achieved on mesh **5**. In Fig. 7 we have reproduced the density levels, the streamlines, the pressure and temperature levels, and the Mach number levels for the simulation on mesh **5**.

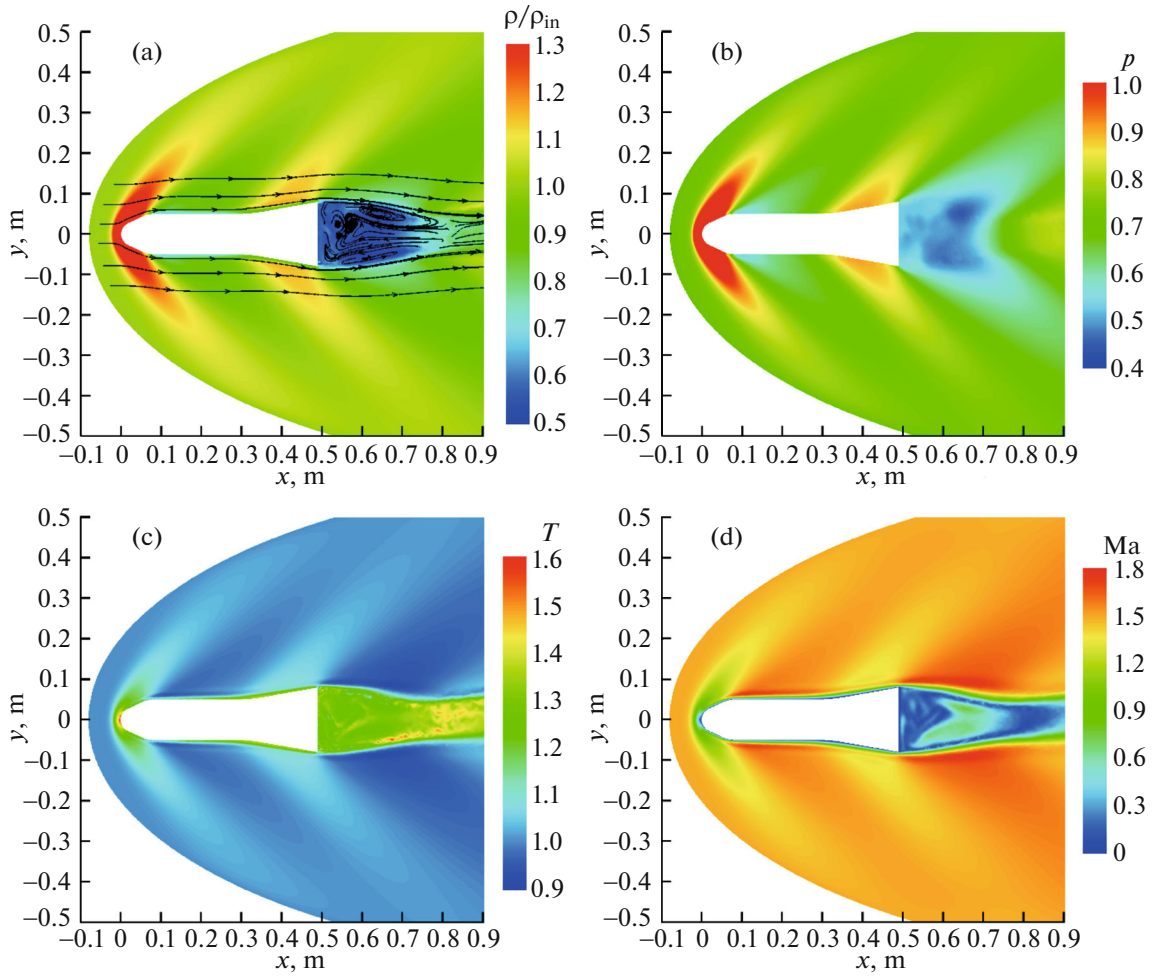

Fig. 7. Density levels and streamlines (a), pressure levels (b), temperature levels (c), and Mach number levels (d) when modeling on mesh **5**.

SUMMARY

Using mesh **5**, which is the best for the totality of parameters (characteristic size of the cells on the surface of the model, degree of non-uniformity, quality of the cells), the best results are obtained in general according to the criteria considered, namely: agreement of the stagnation parameters with theoretical values, agreement of the aerodynamic coefficients and the surface pressure profiles with the experiment, the possibility of modeling the unsteady flow downstream of the base region of the model, and resolution of shocks.

By decreasing the mesh step on the surface, at the cost of increase in the degree of non-uniformity and increase in the cell size away from the model, as well as some deterioration in the cell quality (meshes **1** and **2**), the results in general become worse, and it is not possible to simulate the unsteady regime.

Increasing the degree of mesh uniformity at the cost of increasing the cell size (mesh **6**), the results also become worse than those on meshes **4** and **5**, although the unsteady regime does develop. Therefore, using an almost uniform mesh with a large number of cells is impractical when the mesh step on the model surface is too large. A reasonable choice for the mesh step on the model surface, *hm*, can be roughly estimated to obtain adequate simulation results: $hm < 4$ mm at the diameter $D = 100$ mm of the cylindrical part of the model.

In comparing the results obtained on meshes **1** and **2**, as well as in meshes **3**, **4**, and **5**, it can be seen that in most cases the results improve when the mesh is refined while maintaining the remaining parameters, i.e., mesh convergence takes place.

Note that even on mesh **3**, which has a very small number of cells for simulation of supersonic flow but is balanced in its parameters, it is possible to obtain an approximately accurate flow pattern, but without precise agreement with experiment and without the ability to simulate unsteady flow regime. Calculations on mesh **3** take about an hour of computer time. This can be useful when rapid approximate results are needed.

ACKNOWLEDGMENTS

The authors wish to thank A.G. Churbanov for consultations on the use of the Gmsh package.

FUNDING

This work was supported by ongoing institutional funding. No additional grants to carry out or direct this particular research were obtained.

CONFLICT OF INTEREST

The authors of this work declare that they have no conflicts of interest.

REFERENCES

1. Watson D. F., Computing the *n*-dimensional Delaunay tessellation with application to Voronoi polytopes, *The Computer Journal*, 1981, vol. 24, no. 2, pp. 167–172. https://doi.org/10.1093/comjnl/24.2.167
2. Bowyer A., Computing Dirichlet tessellations, *The Computer Journal*, 1981, vol. 24, no 2, pp. 162–166. https://doi.org/10.1093/comjnl/24.2.162
3. George, P.-L. and Frey, P.J., *Mesh Generation*, Lyon: Hermes, 2000.
4. Rebay S. Efficient unstructured mesh generation by means of Delaunay triangulation and Bowyer–Watson algorithm, *J. Comput. Phys.*, 1993, vol. 106, pp. 25–138. https://doi.org/10.1006/jcph.1993.1097
5. Sukov S. A., *Tetrahedral Mesh Generation Algorithms and Applications*, Moscow: Keldysh Institute of Applied Mathematics of Russian Academy of Science, Preprint no. 23, 2015. Available at http://library.keldysh.ru/preprint.asp?id=2015-23.
6. Poliakov, S.V. and Churbanov, A.G., *Free and Open Source Software for Mathematical Modeling*, Moscow: Keldysh Institute of Applied Mathematics of Russian Academy of Science, Preprint no. 145, 2019. Available at https://library.keldysh.ru/preprint.asp?id=2019-145.
7. Ermakov, M.K. and Kriuchkova, A.S., Generation of unstructured tetrahedral meshes for flow past flight vehicles based on open packages, *Physical–Chemical Kinetics in Gas Dynamics*, 2020, vol. 21, no. 2. https://doi.org/10.33257/PhChGD.21.2.897
8. Shirokov, I.A. and Elizarova, T.G., On the influence of a spatial mesh structure on the results of numerical simulation of a shock wave in a flow around a 3D model, *Fluid Dyn.,* 2022. vol. 57, suppl. 1, no 9, pp. S1–S12. https://doi.org/10.1134/S0015462822601474
9. Gray, J.D., *Summary Report on Aerodynamic Characteristics of Standard Models HB-1 and HB-2,* AEDC-TDR-64-137, 1964.
10. Ceresuela, R., *Maquettes etalons HB-1 et HB-2. Caracteristiques aerodynamiques mesurees dans les souffleries de l'O.N.E.R.A. de Mach 2 a Mach 16.5*, Note Technique O.N.E.R.A., 1968, no. 123.
11. Vukovic, Dj. and Damljanovic, D., HB-2 high-velocity correlation model at high angles of attack in supersonic wind tunnel tests, *Chinese Journal of Aeronautics*, 2019, vol. 32(7), pp. 1565–1576. https://doi.org/10.1016/J.CJA.2019.03.022
12. Kryuchkova, A.S., Numerical simulation of supersonic flows over ballistic models using UST3D programming code, *Physical-Chemical Kinetics in Gas Dynamics*, 2018, vol. 19, no. 4. https://doi.org/10.33257/PhChGD.19.4.783
13. Chetverushkin, B.N., *Kinetic Schemes and Quasi-Gas Dynamic System of Equations*, Barselona: CIMNE, 2008.
14. Elizarova, T.G., *Quasi-Gas Dynamic Equations*, Dordrecht: Springer, 2009. https://doi.org/10.1007/978-3-642-00292-2
15. Sheretov, Yu.V., *Regularized Hydrodynamic Equations*, Tver: Tver State University, 2016.
16. Elizarova, T.G., Graur, I.A., Lengrand, J.C., and Chpoun, A., Rarefied gas flow simulation based on quasi gas dynamic equations, *AIAA J.*, 1995, vol. 33, no. 12, pp. 2316–2324.
17. Elizarova, T.G. and Shirokov, I.A., *Regularized Equations and Examples of Their Use in the Modeling of Gas-Dynamic Flows*, Moscow: MAKS Press, 2017.

18. Shirokov, I.A. and Elizarova, T.G., Simulation of laminar–turbulent transition in compressible Taylor–Green flow basing on quasi-gas dynamic equations, *J. of Turbulence*, 2014, vol. 15, no. 10, pp. 707–730. https://doi.org/10.1080/14685248.2014.927581
19. Elizarova, T.G. and Shirokov, I.A., Artificial dissipation coefficients in regularized equations of supersonic aerodynamics, *Doklady Mathematics*, 2018, vol. 98, no. 3, pp. 648–651. https://doi.org/10.1134/S1064562418070141
20. Shirokov, I.A., *Numerical study of the aerodynamic characteristics of a triangular wing at different angles of attack and large Mach numbers*, Moscow: Keldysh Institute of Applied Mathematics of Russian Academy of Science, Preprint no. 56, 2021. Available at https://library.keldysh.ru/preprint.asp?id=2021-56.
21. *TetGen: A Quality Tetrahedral Mesh Generator*. Available at http://tetgen.berlios.de.
22. *Gmsh: Three-Dimensional Finite Element Mesh Generator*. Available at https://gmsh.info.
23. Shirokov, I.A., Mesh construction algorithm based on TetGen for modeling the external flow around an axisymmetric model, *Mathematical Models and Computer Simulations*, 2021, vol. 13, no. 6, pp. 1148–1159.
24. K-100 System, Keldysh Institute of Applied Mathematics RAS, Moscow. Available at https://www.kiam.ru/MVS/resourses/k100.html.

Translated by E.A. Pushkar